Transport processes of uniform and mixed sands in oscillatory sheet flow

3 authors, including:

Wael Neiazy Hassan
Ghent University
25 PUBLICATIONS **336** CITATIONS

ELSEVIER

Transport processes of uniform and mixed sands in oscillatory sheet flow

Wael N. Hassan [a,*], Jan S. Ribberink [b]

[a]*Hydraulics Research Institute, National Water Research Center, Delta Barrage 13621, Egypt*
[b]*Water Engineering and Management, Faculty of Engineering, University of Twente, PO Box 217, 7500 AE, Enschede, The Netherlands*

Abstract

New experiments were carried out in the Large Oscillating Water Tunnel of WL|Delft Hydraulics (scale 1:1) using asymmetric 2nd-order Stokes waves. The main aim was to gain a better understanding of size-selective sediment transport processes under oscillatory plane-bed/sheet-flow conditions. The new data show that for uniform sand sizes between $0.2 < D < 1.0$ mm, measured net transport rates are hardly affected by the grain size and are proportional to the third-order velocity moment. However for finer grains ($D = 0.13$ mm) net sand transport rates change from the 'onshore' direction into the 'offshore' direction in the high velocity range. A new measuring technique for sediment concentrations, based on the measurement of electro-resistance (see [McLean, S.R., Ribberink, J.S., Dohmen-Janssen, C.M. and Hassan, W.N.M., 2001. Sediment transport measurements within the sheet flow layer under waves and currents. J. Waterw., Port, Coast., Ocean Eng., ISSN 0733-950X]), was developed further for the improved measurement of sediment dynamics inside the sheet-flow layer. This technique enabled the measurements of particle velocities during the complete wave cycle. It is observed that for long period waves ($T = 12.0$ s), time-dependent concentrations inside the sheet-flow layer are nearly in phase with the time-dependent flow velocities. As the wave period decreases, the sediment entrainment from the bed as well as the deposition process back to the bed lags behind the wave motion more and more. The new data show that size-gradation has almost no effect on the net total transport rates, provided the grain sizes of the sand mixture are in the range of $0.2 < D < 1.0$ mm. However, if very fine grains ($D = 0.13$ mm) are present in the mixture, net total transport rates of graded sand are generally reduced in comparison with uniform sand with the same D_{50}. The transport rates of individual size fractions of a mixture are strongly influenced by the presence of other fractions in a mixture. Fine particles in sand mixtures are relatively less transported than in that uniform sand case, while the opposite occurs for coarse fractions in a mixture. The relative contribution of the coarse grains to the net total transport is therefore larger than would be expected based on their volume proportion in the original sand mixture. This partial transport behaviour is opposite to what is generally observed in uni-directional (e.g. river) flows. This is caused by vertical sorting of grain sizes in the upper bed layer and in the sheet flow and suspension layers. Kinematic sorting is believed to be responsible for the development of a coarse surface layer on top of a relatively fine sub-layer, providing in this way a relatively large flow exposure for the coarser sizes. Furthermore fine grains are suspended more easily than coarse grains to higher

---

* Corresponding author. Tel.: +31 53 4897453; fax: +31 53 4895377.
  E-mail address: wnmhassan@gmail.com (W.N. Hassan).

elevations in the flow where they are subject to increasing phase-lag effects (settling lags). The latter also leads to reduced net transport rates of these finer sizes.

1. Introduction

Field observations show that sea bed sediments are hardly ever uniform, but are generally composed of a mixture of different grain sizes (Katoh and Yana-gishima, 1995; Guillen and Hoekstra, 1997). For example, the Dutch coast consists mainly of sand with median grain size in the range of 125–600 μm. Besides, field observations show the existence of sorting of sediment grains along the cross-shore profile with coarse material generally present near the shore-line and fine material in deeper water (see Guillen and Hoekstra, 1997). Coastal cross-shore profiles show strong correlations between morphology (bars) and sediment composition of the seabed. It also known from beach profile observations that grain size is an important parameter for the shape of the beach profile (Dean, 1991). Until now, little attention is paid to grain-size sorting and its underlying selective transport mechanisms. Besides, the effect of sediment size-gradation on the transport processes under wave conditions is still not investigated. There are several reasons to pay more attention to the influence of sediment characteristics (e.g. size, gradation) on the sediment transport processes. Beach or shoreface nourishments are generally carried out with different (dredged) materials than the sand as currently present. However, not much is known about the possibilities of using different bed materials (deviating from the present coastal profile) for the design of effective beach nourishments schemes.

Existing coastal morphological models are not able to account for spatial and temporal variations in grain size and gradation. This is mainly caused by the fact that there is a lack of basic knowledge about sediment transport processes of graded sediments in wave-dominated conditions. As a result no sediment transport models are available which are able to compute magnitudes as well as size composition of transported sediments. In a pioneering study Van Rijn (1997a) explored cross-shore sorting of sediment mixtures using a process-based model (CROSMOR) provided with a single and a multi-size-fraction approach. Van Rijn found that calculated bed-load transport rates of sediments between 0.2 and 0.8 mm are slightly to significantly larger when a multi-fraction method is used in stead of a single-fraction method. Besides, the suspended-load transport rates of the multi-fraction method are significantly smaller than those of the single-fraction method at small current velocities.

Most studies on sand transport processes of graded sands were carried out for uni-directional flows (river field). Experiment studies of selective transport processes in uni-directional flows were for example carried out by Wilcock (1993), Wilcock et al. (2001), Blom et al. (2003) and Kleinhans (2004). Due to vertical sorting effects and bed form dynamics, finer particles are generally dominating in the upper bed layers, while coarser particles are dominating the lower bed layers. This leads to a kind of stratified bed and consequently to a different flow exposure of the various sizes. There is still hardly any knowledge about the occurrence and the possible mechanisms of vertical bed sorting under wave conditions.

The present paper is aimed at studying selective sediment transport processes of graded sediments under strong waves over plane beds in the sheet-flow regime. In the near-shore zone plane, sea beds/ sheet flow occur when the wave-induced bed-shear stresses become so large that the Shields parameter reaches values in the range $\theta > 0.8$. During storm conditions this is generally the case for most of the upper shoreface, for more moderate wave conditions plane beds are present in the shoaling area just before the breaking point. Also in the swash zone on the beach plane beds are observed. The transition from rippled-beds to plane beds ($\theta > 0.8$, Wilson, 1987) involves a drastic drop of the sediment mixing capacity of the flow. Sediment suspension in the water column is no longer dominated by vortex shedding around bed ripples (Ribberink and Al-Salem, 1994). Sand is mainly transported as 'sheet flow' in a thin

layer above the sea bed with high sand concentrations (thickness of order 1 cm) and high transport rates. Intergranular forces and grain–water interactions become important with these high concentrations.

Under these severe conditions it is difficult to perform field measurements. Therefore most of the available studies on sheet flow are carried out in oscillatory flow tunnels in which the wave-induced oscillatory flows near the sea bed can be simulated, e.g. King (1991), Dibajnia and Watanabe (1992, 1996, 2000), Ribberink and Al-Salem (1994, 1995), Zala Flores and Sleath (1998), Watanabe and Sato (2002).

Dohmen-Janssen et al. (2001, 2002) showed that grain size has a significant effect on sediment transport processes in oscillatory sheet flows with a superimposed net current. Dibajnia and Watanabe (1996, 2000) showed with oscillatory sheet-flow experiments that the transport rates of fine grains in a mixture are affected by the presence of coarse grains. Recently, Ahmed and Sato (2003) and O'Donoghue and Wright (2004) show with detailed sheet-flow measurements that velocities and concentrations in the sheet-flow layer are strongly affected by grain size as well as by sediment gradation.

Despite these pioneering studies there is still a lack of experimental data of transport rates, concentrations and velocities in sheet-flow conditions for various oscillatory flows and for various mixtures of grain sizes sediments.

In the present paper the results of a series of new oscillatory sheet-flow experiments with uniform and graded sediments will be presented, based on research as carried out during the preceding years in the Large Oscillating Water Tunnel of WL|Delft Hydraulics. The emphasis of the experiments lies on (i) the behaviour of net transport rates of individual size fractions in a mixture, (ii) how total net transport rates are affected by sediment grain size and gradation, and (iii) which segregation mechanisms may be responsible for the observed transport behaviour. Moreover, by using an improved measuring technique for sediment concentrations and grain velocities in the sheet-flow layer (McLean et al., 2001), additional insights are obtained in intra-wave sheet-flow dynamics.

2. Experimental set-up and the measuring programme

2.1. The large oscillating water tunnel

The experiments were carried out in the Large Oscillating Water Tunnel (LOWT) of WL|Delft Hydraulics (for a description see Ribberink and Al-Salem, 1994). The tunnel enables a full-scale simulation of wave-induced oscillatory flows near the sea bed (see Fig. 1 for a general outline of the tunnel). The tunnel has a vertical U-tube shape, with a long horizontal rectangular test section. The piston motion induces the desired horizontal orbital wave motion close to the bed. The maximum piston amplitude is 0.75 m, which results in a maximum semi-excursion
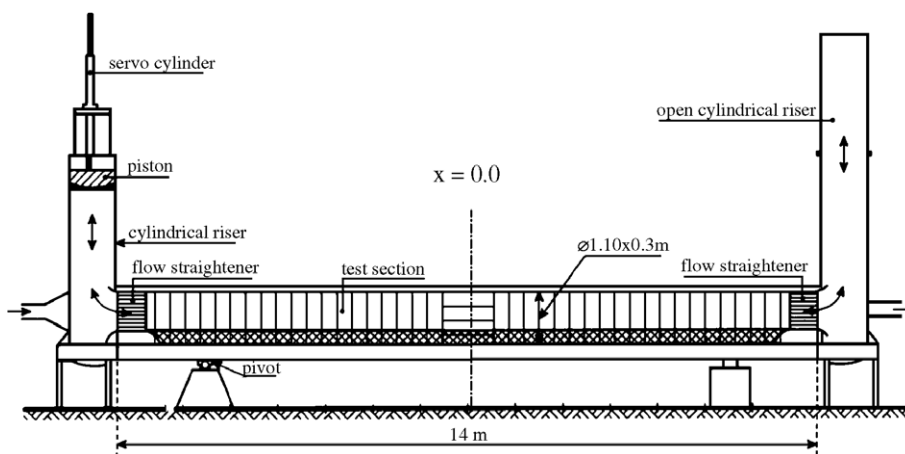

Fig. 1. General outline of the Large Oscillating Water Tunnel (LOWT) of WL|Delft Hydraulics.

length of the water particles in the test section of 2.45 m. The range of the velocity amplitudes is 0.2–1.8 m/s and the range of oscillating periods is 4–15 s.

The test section has a length of 14 m, a height of 1.1 m, a width of 0.3 m and is provided with flow straighteners at each end. A 0.3-m-thick layer of sand is brought into the test section, so 0.8 m height is left for the oscillating water flow. At the bottom of both vertical tubes, sand traps are constructed to collect the sand that leaves the test section during a test. The wave tunnel is also provided with a recirculating flow system, which enables the superposition of a net current on the oscillating motion.

2.2. Sand bed

The new LOWT experiments were carried out with different uniform and graded sands. Basically four uniform sands were used with $D_{50}=0.13$, 0.21, 0.34 and 0.97 mm, which were mixed in different proportions for the graded-sand experiments. All sands are composed primarily of angular quartz grains and have the same density (2650 kg/m^3). Grain-size distributions of the 'uniform' sands and of the composed mixtures are shown in Fig. 2. Table 1 shows the main grain-size characteristics of these sands and the correspondent series of experiments. In this table D_i denotes the diameter at which i% by weight is finer; w_s

Table 1
Characteristics of all sands as used in the LOWT experiments

Sand type	D_{10} (mm)	D_{50} (mm)	D_{90} (mm)	σ_g	w_s (mm/s)	Series
Uniform	0.15	0.21	0.29	1.29	26.0	B, C
	0.10	0.13	0.18	1.30	11.4	D, O
	0.23	0.34	0.39	1.28	43.8	R
	0.85	0.97	1.20	1.32	110.0	Q
Graded	0.16	0.24	0.99	2.67	33.0	P
	0.11	0.15	1.08	4.21	12.5	S
	0.097	0.194	0.406	1.85	20.3	K

Series names are used as in the original data reports.

is the median settling velocity of the sand in still-water and σ_g is the geometric standard deviation, defined as:

$$\sigma_g = 0.5\left(\frac{D_{50}}{D_{16}} + \frac{D_{84}}{D_{50}}\right). \tag{1}$$

From the four basic uniform sands sizes the following three sand mixtures were composed. Sand mixture P consists of 30% of coarse 0.97 mm sand and 70% of medium 0.21 mm sand. Sand mixture S consists of 20% of coarse 0.97 mm sand, 20% of medium 0.34 mm sand and 60% of fine 0.13 mm sand. Sand mixture K consists of 50% fine 0.13 mm sand and 50% of medium 0.34 mm sand. These (artificial) bi-modal and tri-modal sand mixtures were selected to (i) enable a comparison with earlier uniform sand experiments in which the same basic sizes were used, and (ii) to facilitate the grain-size
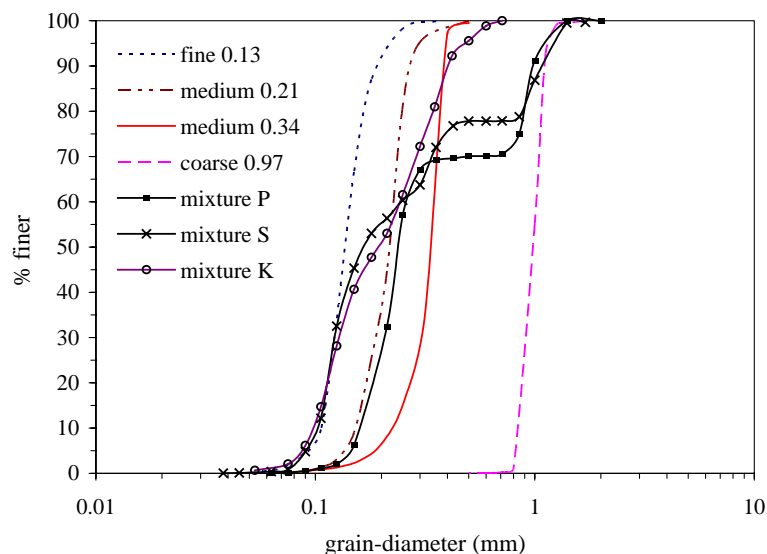

Fig. 2. Grain-size distributions of the 'uniform' and 'graded' sands as used in the LOWT experiments.

analysis of sand samples during the experiments. Although uni-modal sand mixtures are more common in nature, multi-modal mixtures can still be of some practical relevance in the framework of for example beach nourishment situations.

The set-up of the experiments with uniform sand is in line with the previous LOWT series by Al-Salem (series B, C 1993) and Ribberink and Chen (series D, 1993). The data of series B, C ($D_{50} = 0.21$ mm) were published by Ribberink and Al-Salem (1994), the data of series D (0.13 mm) are included in the present paper. New uniform sands with $D_{50} = 0.34$ and 0.97 mm were selected for the present new experiments in order to extend the existing data-base in the 'coarse' direction.

2.3. Hydraulic conditions

To obtain a set of comparable data for uniform and graded sands, the experiments were mainly carried out with asymmetric 2nd-order Stokes waves (see also Al-Salem (1993). The time-dependent velocity of 2nd-order Stokes wave can be described with: $u(t) = u_1 \cos(\omega t) + u_2 \cos(2\omega t)$, where: u_1 and u_2 represent the velocity amplitude of respectively the 1st- and 2nd-order component of the horizontal orbital flow and ω = the angular frequency of the wave (= $2\pi / T$, T = wave period). Tables 2 and 3 provide an overview of the hydraulic conditions during all LOWT-experiments with uniform and graded sands as used in the present study. In these tables, the root-mean-square velocity $U_{rms} = [\frac{1}{2}(u_1^2 + u_2^2)]^{0.5}$, the crest velocity $U_c = u_1 + u_2$, the trough velocity $U_t = u_1 - u_2$. The degree of asymmetry R, defined as $U_c / (U_c + U_t) = (u_1 + u_2)/2u_1$, was kept around 0.65. The wave period T was varied in a limited number of tests, to study the influence of time-dependency and flow acceleration.

During series O, which is aimed at detailed measurements of sheet-flow dynamics, sine waves (velocity amplitude $u_1 = 1.1$ m/s) with a superimposed net current ($\langle u \rangle = 0.25$ m/s) were used, in order to enable a

Table 2
Hydraulic conditions of all series of experiments with uniform sands

Series	Test	Hydraulic conditions						D_{50} (mm)
		Wave cycle	U_{rms} (m/s)	U_c (m/s)	U_t (m/s)	Period T (s)	Wave type	
B	B7	Full	0.50	0.95	0.5	6.5	2nd-order Stokes	0.21
	B8		0.70	1.31	0.7			
	B9		0.92	1.72	0.86			
C	C1	Full	0.55	1.07	0.57			0.21
	C2		0.55	1.11	0.54			
	C9		0.56	1.05	0.66			
	C11		0.80	1.39	0.87			
D	D11	Full	0.56	1.00	0.59			0.13
	D12		0.91	1.60	0.94			
	D13		0.73	1.30	0.76			
	D14		0.45	0.79	0.48			
O	O4	Full	0.82	1.36	0.85	7.2	Sine + current	0.13
	O7		0.83	1.39	0.87	4.0	(0.25 m/s)	
	O12		0.82	1.37	0.83	12		
R	R1	Full	0.59	1.07	0.58	6.5	2nd-order Stokes	0.34
	R2		0.68	1.22	0.66			
	R3		0.89	1.57	0.84			
	R4		0.68	1.20	0.72	5		
	R5		0.67	1.15	0.69	12		
Q	Q6c	Crest	0.72	1.14		2.75		0.97
	Q7c		0.85	1.34				
	Q9c		1.08	1.64				
	Q6t	Trough	0.50		0.67	3.75		
	Q7t		0.57	0.77				
	Q9t		0.73	1.02				

Series names and test numbers are used as in the original data reports.

Table 3
Hydraulic conditions of all series of experiments with graded sands

Series	Test	Hydraulic conditions						Sand mixture
		Wave cycle	U_{rms} (m/s)	U_c (m/s)	U_t (m/s)	Period T (s)	Wave type	
K	K1	Full	0.84	1.54	0.78	6.5	2nd-order Stokes	50% of 0.21 mm+50% of 0.32 mm
	K2		0.58	1.10	0.55			
P	P1		0.59	1.08	0.57	6.5		70% of 0.21 mm+30% of 0.97 mm
	P2		0.64	1.23	0.64			
	P3		0.85	1.59	0.85			
S	S1		0.45	0.87	0.45			60% of 0.13 mm+20% of 0.34 mm+
	S2		0.61	1.14	0.57			20% of 0.97 mm
	S3		0.70	1.30	0.65			
	S4		0.90	1.63	0.82			
	S5		0.67	1.17	0.67	12		

Series names and test numbers are used as in the original data reports.

comparison with the previous similar experiments of McLean et al. (2001).

For series Q (with coarse 0.97 mm sand) instead of imposing a series of full asymmetric wave cycles, separate series of half (crest and trough) cycles were imposed (see also King, 1991) in order to avoid the growth of large ripples and keep the bed flat and in the sheet-flow regime. In this way large measurable transport rates could be realized in a short measuring period, being short enough to avoid bed form growth. Basic underlying assumption of these half-cycle tests is that the coarse 0.97 mm sand behaves in a 'quasi-steady' manner during the wave cycle and unsteady transport phenomena, associated with time-evolution of the boundary layer and vertical sediment exchange with the bed (time-history effects), are negligible. Justification for this is given by Dohmen-Janssen et al. (2002), who compare 'quasi-steady' and 'unsteady' sheet-flow models and conclude that unsteady effects become important for sizes finer than about 0.2 mm. Under this assumption, the net transport of full asymmetric wave cycles can be obtained by subtracting the net transported sediment volumes of separate 'crest' and trough half-cycles.

2.4. Measuring techniques/instruments and procedure

The different measuring instruments and techniques that have been used during the present series of experiments are presented in Table 4.

Net sediment transport rates were measured with a mass-conservation technique by measuring sand volume changes in the test section in combination with weight measurements of sand collected in two sand

Table 4
Measured parameters and measuring techniques/instruments

Measured parameter	Measuring technique/instrument	Used in series
Net (half or full-cycle averaged) sediment transport rates	Mass Conservation Technique (MCT) with sand traps and bed-level profiling (PROVO)	B, C, D, P, Q, R and S
Oscillatory flow velocity above the boundary layer	2DV Laser-Doppler system (LDA) at 10–20 cm above the sand bed	B, C, D, P, Q, R and S
Time-averaged suspended sediment concentration profiles	Transverse Suction System (TSS)	P and S
Half-cycle mean sediment concentrations in the sheet-flow/bed-load layer	Pumping Bed-load Trap sampler (PBLT)	P, R and S
Time-dependent concentrations and grain velocities in the sheet-flow layer	Conductivity Concentration Meter (CCM)	O
Bed sampling/cores	Bed Sampler (BS)	P and S
Grain-size distributions of bed samples, PBLT samples, sand trap samples and TSS samples	Settling velocity analysis (VAT)	P, R and S

traps at both ends of the test section. Since the tunnel was not provided with an 'upstream' sand feeding arrangement, a bed erosion wave migrated slowly into the tunnel and also the size composition of the upper sand layer changed slowly during a tunnel run. In order to avoid that this boundary effect would influence the measurements, (i) the test duration was kept short (less than 12 min), (ii) after each test (with graded sand) the upper bed layer with a thickness of ca. 5 cm was removed and replaced by a new undisturbed mixture, and (iii) the test section bed was flattened (filling up erosion holes). For each wave condition three or four tests were carried out in order to achieve a more accurate measurement of the net sediment transport rate.

Sand volume changes in the test section were measured by carrying out bed-level measurements along the complete test section before and after each tunnel test using a bed-level profiling system (PROVO). The system consists of three bed profilers, positioned on a measuring carriage at different positions in the cross-section, which can move along the test section. A shaft encoder and position counter are used to determine the horizontal position of the profilers along the test section. The PROVO system is based on conductivity measurements and designed such that the conductivity in the sampling volume at the probe tip is kept constant. A control unit uses this conductivity information to keep the probe tip at a constant distance from the sand bed. The vertical elevation of the probe tip is measured with a potentiometer system (see Hassan, 2003).

A 2D-forward scatter Laser-Doppler Anemometer (LDA) was used to measure time-dependent flow velocities in the vertical plane along the test section above the wave boundary layer (for a description of the LDA system, see Klopman, 1994). The LDA has a small sampling volume, with a height and width (in flow direction) of 0.22 mm. The LDA was not able to measure flow velocities close to the bed ($z < 100$ mm), because of the blockage of the laser beams by sediment particles.

Two Conductivity Concentration Meters (CCM) were used to measure time-dependent concentrations and particle velocities in the sheet-flow layer. The CCM measures high concentrations (100–1600 g/l) with a four-point electro-resistance method (see Ribberink and Al-Salem, 1995). The measured signal is proportional to the electro-resistance of the sand–water mixture in a small sensing volume directly above the electrodes. The two CCMs were installed through the tunnel bottom in order to avoid large flow disturbance and penetrated the sheet-flow layer from below. They were positioned at a distance of 11 mm (along the test section) in order to be able to apply the cross-correlation technique (see Section 4.3).

Time-averaged suspended sand concentrations were measured using a Transverse Suction System (TSS, see Bosman et al., 1987). Water–sediment samples are extracted in a direction normal to the flow direction. The system consists of 10 separate intake nozzles above each other, covering a vertical distance of 26 cm, enabling the measurement of a complete concentration profile during one measurement run. The nozzles have an inner diameter of 3 mm and are positioned at small distance near the bed (1 cm) and at larger distance (6 cm) far above the bed.

A Pump Bed-Load Trap sampler (PBLT, see Van Rijn, 1997b) was used to measure half wave cycle ('onshore' and 'offshore') average sediment concentrations in the sheet-flow layer. An average result is obtained by using the sampler for 2 min during a tunnel test. The PBLT consists of two tube-type intake nozzles placed in opposite direction on a metal footplate (length of about 0.1 m, width of about 0.05 m) as shown in Fig. 3. Each nozzle is connected to a plastic hose for extracting water and sediment and has internal diameter of 8 mm, which exceeds the sheet-flow layer thickness. In this way the complete sediment transport layer is sampled. The nozzles are opened and closed alternatively by circular metal valves (with rubber cover) through the action of oscillatory fluid drag on a metal pivoting plate connected by thin steel rods to the valves. The valve of the nozzle facing the forward (onshore) fluid motion is open during the forward stroke of the wave and is closed during the backward stroke. At the same time the other valve, facing the backward motion, is respectively closed and open. The intake nozzle facing the forward motion will be referred to as the 'onshore' nozzle, while the one facing the backward motion is referred to as the 'offshore' nozzle.

A Bed Sampler (BS) was used to take small core samples out of the sand bed at different positions along the tunnel after a tunnel run, to measure vertical profiles of grain-size composition in the upper layer of the sand bed (vertical sorting). The BS, consisting of a perspex cylinder with inner diameter 25 mm and a height of
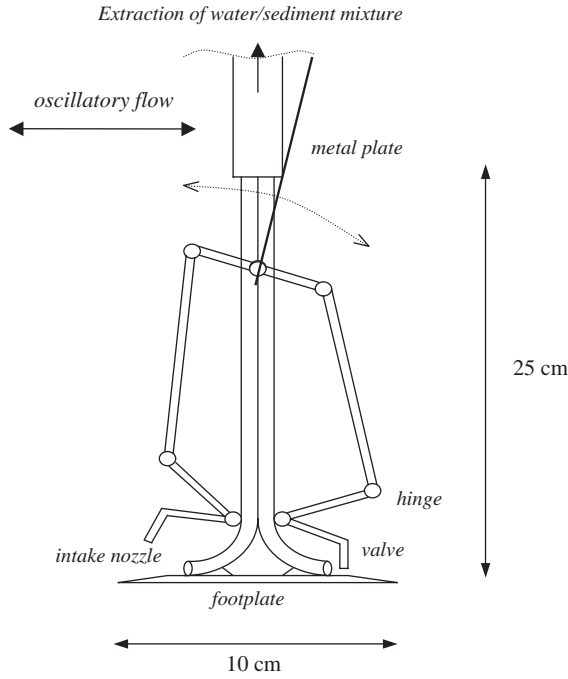
Fig. 3. General outline of the Pump Bed-Load Trap sampler (PBLT).

about 100 mm, is carefully pushed into the sand bed. For each test, bed samples were taken at 3 to 5 positions along the tunnel before and after tunnel runs. The upper 9 to 50 mm of the samples were divided into different subsamples with a thickness of about 3 to 10 mm each.

The grain-size compositions of all sand samples, as collected by TSS, PBLT and BS, were determined with a settling tube. The multi-modal character of the used sand mixtures made it possible to measure size-fraction percentages (of 2–3 fractions) in a (relatively) efficient way.

3. Methods of data analysis

3.1. Net total transport rates

Net sand transport rates along the tunnel are calculated by integration of the sediment continuity equation, starting at the right- and at the left boundary of the test section and making use of the measured bed-level changes along the test section. The boundary conditions are provided by the sand trap measurements. In this way for each test two estimates of the

net sand transport rate can be obtained at each position in the test section as follows:

$$q_{s,1} = \frac{\Delta V_{1,\mathrm{ip}}(1 - \varepsilon_0)}{\Delta t W} - \frac{G_1}{\rho_s} \times \frac{1}{\Delta t W}$$

left trap estimate   (2)

$$q_{s,r} = \frac{-\Delta V_{r,\mathrm{ip}}(1 - \varepsilon_0)}{\Delta t W} + \frac{G_r}{\rho_s} \times \frac{1}{\Delta t W}$$

right trap estimate   (3)

where $\Delta V_{1,\mathrm{ip}}$=total eroded volume, including pores, from the part of the tunnel test section left of the measurement location and $\Delta V_{r,\mathrm{ip}}$=total eroded volume, including pores, from the part of the tunnel test section right of the measurement location; G_1=total (dry) weight of the sand collected in the left trap (underneath the piston); G_r=total (dry) weight of the sand collected in the right trap (underneath the open cylindrical riser); ρ_s=density of sand (2650 kg/m^3); ε_0=porosity of sand bed=0.4; W=width of tunnel test section=0.3 m; q_s=net transport rate without pores per unit width and time; Δt=test duration.

The measured transport rate for each test is generally based on the average value of both estimates $(q_{s,1}+q_{s,r})/2$ in the middle of the test section, where the conditions are not disturbed by the test section boundaries. Finally, these measured transport rates per test are averaged over 3–4 repetitive tests.

For the half-cycle experiments (series Q), separate transport measurements are carried out for the 'crest' experiments and for the 'trough' experiments, respectively, $q_{s,c}$ and $q_{s,t}$. The net transport rates q_s for the full wave cycle are calculated as follows:

$$q_s = \frac{1}{T}\{T_c\, q_{sc} + T_t\, q_{st}\} \qquad (4)$$

where T_c=duration of the crest half wave cycle, T_t=duration of the trough half wave cycle and $T=T_c+T_t$=wave period.

3.2. Net sand transport rates of each size fraction

Net transport rates of each size fraction were calculated using the measured net total transport rates in combination with the size composition of the sand

samples extracted with the PBLT. The measured time-averaged 'onshore' and 'offshore' concentrations C_{on} and C_{off} of the PBLT are used to estimate the 'onshore' and 'offshore' bed-load transport rates as follows (Van Rijn, 1997b):

$$q_{b,on} = \alpha d C_{on} U_{max,on}, \quad q_{b,off} = \alpha d C_{off} U_{max,off} \quad (5)$$

where: α=calibration factor; d=internal diameter of intake nozzle (= 0.008 m) and $U_{max,on/off}$='onshore' or 'offshore' peak velocity in the free stream (ca. 0.1 m above the bed).

The net total bed-load transport for the full wave cycle is then:

$$q_{b,net} = \alpha D \big(C_{on} U_{max,on} T_{crest} - C_{off} U_{max,off} T_{trough} \big) / T \quad (6)$$

in which T_{crest}=duration of the wave crest; T_{trough}= duration of the wave trough and T=total wave period (= $T_{crest} + T_{trough}$).

The calibration factor α accounts for scour effects around the PBLT, variable thickness of the sheet-flow layer and variable velocity and concentration profiles across the intake nozzles. The PBLT calibration factor α is determined using Eq. (6) in combination with the net total transport rates as measured with the mass-conservation technique. Van Rijn (1997b) calibrated the PBLT in the LOWT during separate uniform sand (D=0.21 mm) experiments, using net transport rates as measured earlier by Al-Salem (1993). Using the data of Van Rijn (1997b) and the present experiments, it was found that α is inversely proportional to the time-averaged bed-load concentration, $\alpha = 5.37\langle c \rangle^{-0.8}$. The calibration factor α varied between 0.2 and 0.8 for all tunnel data with uniform and graded sands under 2nd-order Stokes wave conditions (see Tables 1, 2 and 3). Small values of α were found in cases with small net transport rates and large time-averaged sand concentrations in the flow (cases with fine sand D=0.13 mm). In fact, large time-averaged concentrations do not always lead to large net transport rates like in uni-directional flow. Unsteady effects in oscillatory flows can play an important role and control the magnitude and the direction of the net transport rates. Net transport rates of each size fraction are also calculated using Eq. (6), but now replacing the total concentrations C_{on} and C_{off} by the concentrations of each size fraction.

3.3. Sand concentrations and particle velocities inside the sheet-flow layer

The measured signals of the two CCM sensors are translated into concentrations using available calibration factors (see Hassan, 2003). Ensemble-averaged concentrations are first computed for each CCM probe individually and the mean result of the two probes is used as the final measured result. In general the concentrations at each elevation were ensemble-averaged for more than 25 waves. The measured time series of the two CCM sensors were also used to calculate the time-dependent grain velocities inside the sheet-flow layer with a cross-correlation technique (see McLean et al., 2001; Hassan, 2001, 2003). Hereto the wave period was divided into 36 intervals and for each interval cross-correlations between the two time series were calculated for different time-shifts around the center point of each interval.

Typical plots of ensemble-averaged cross-correlations versus time lag are shown in Fig. 4 for condition O4. The upper panel shows the measured velocity (by LDA) at 100 mm above the bed, the middle panel (A) shows the cross-correlations during the crest part of the wave cycle while the lower panel (B) shows the trough part. The numbers on the right hand side indicate wave phase/interval number. Phase 1 occurs just after flow reversal from trough to crest direction (upward zero crossing) and phase 36 just before the flow reversal (downward zero crossing). For clarity, the traces of the cross-correlation for each phase are displaced vertically. Even though the correlation maximum is often small (sometimes less than 0.05), the pattern is clear. The velocity of the sediment particles is given by $u=\Delta x / \Delta t$, where Δt is the time-shift of the maximum correlation from the zero lag line and Δx is the distance between the CCM probes (= 11 mm).

4. Results of the uniform sand experiments

4.1. Measured net transport rates

All measured net transport rates with uniform sands are summarised in the Tables 5–8. These data include series Q (D_{50}=0.97 mm), series R (D_{50}=0.34 mm), series B and C (D_{50}=0.21 mm)
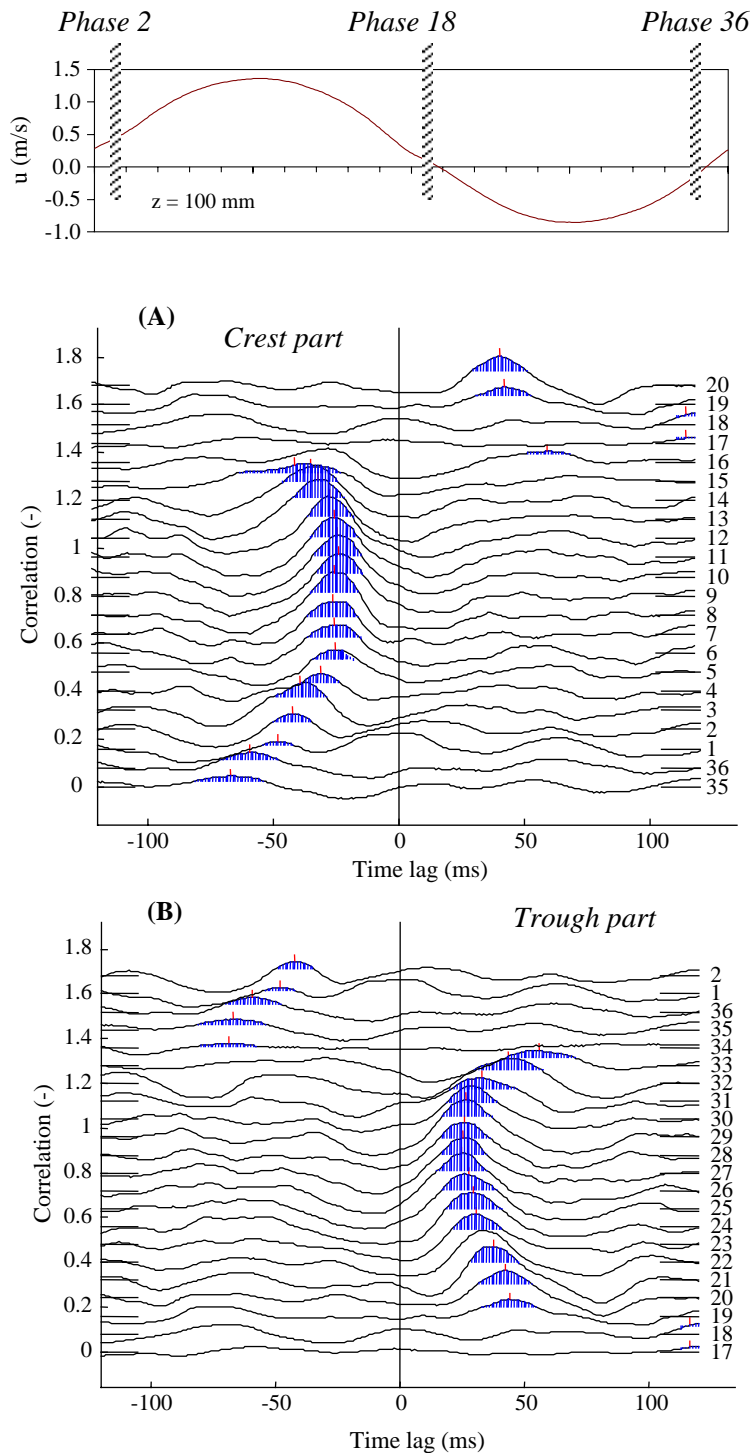
Fig. 4. Ensemble-averaged cross-correlations of two CCM sensors versus time lag ($z = -0.5$ mm, condition O4). The numbers at the right indicate the wave phase, numbered from 1 to 36.

Table 5
Measured net transport rates of series Q with uniform sand (D_{50}=0.97 mm)

Test	T (s)	U_{laser} (m/s)			$\langle U^3 \rangle$ (m³/s³)	$q_s \pm \sigma$ (10^{-6} m²/s)	q_s (10^{-6} m²/s) of the full-wave
		U_c	U_t	U_{rms}			
Q6c	2.75	1.14		0.72	0.490	52.6 ± 1.5	27.12
Q6t	3.75		0.67	0.50	0.140	6.6 ± 2.2	
Q7c	2.75	1.34		0.85	0.807	79.1 ± 20.1	44.67
Q7t	3.75		0.77	0.57	0.215	9.4 ± 0.6	
Q9c	2.75	1.64		1.08	1.645	162.8 ± 31.1	75.66
Q9t	3.75		1.02	0.73	0.444	14.2 ± 3.1	

In the test codes Q refers to the series name, followed by a number referring to U_{rms} of the flow (full-wave), c to wave crest and t to wave-trough.

of Al-Salem (1993) and series D (D_{50}=0.13 mm), respectively. A mean values were determined by averaging the results of different tests. For series Q the measured net transport rates of each half-cycle of the wave are also presented. These tables include also data on the flow characteristics, measured by LDA at $z \geq 0.1$ m above the bed. Each table includes the following: name of test condition, oscillation period T, velocities of asymmetric oscillatory flow, i.e. maximum velocity in crest direction U_c, maximum velocity in trough direction U_t, root-mean-square value of the flow velocity during the wave cycle U_{rms}, time-averaged value of the third power of the velocity $\langle U^3 \rangle$, average net transport rate per unit width $\langle q_s \rangle$, standard deviation σ of the mean net transport rate. Fig. 5 shows the measured net transport rates of series Q (coarse sand, D_{50}=0.97 mm) as a function of $\langle U^3 \rangle$. The figure also includes the half-cycle averaged transport rates of both the crest part (Δ) and the trough part ($\square$) of the wave cycle. It is clear that due to the wave asymmetry the crest part of the wave cycle has much higher velocities, hence higher $\langle U^3 \rangle$ and transport rates are found (about factor 10 higher). It is shown that the measured net transport rates as well

Table 6
Measured net transport rates of series R with uniform sand (D_{50}=0.34 mm)

Test	T (s)	U_{laser} (m/s)			$\langle U^3 \rangle$ (m³/s³)	$q_s \pm \sigma$ (10^{-6} m²/s)
		U_c	U_t	U_{rms}		
R1	6.5	1.07	0.58	0.59	0.129	20.8 ± 1.1
R2		1.22	0.66	0.68	0.204	29.9 ± 1.2
R3		1.57	0.84	0.89	0.450	77.1 ± 5.9
R4	5.0	1.20	0.72	0.68	0.184	38.2 ± 2.5
R5	12.0	1.15	0.69	0.67	0.155	24.4 ± 1.6

as the measured transport rates per half wave cycle show more or less a linear relation with the third-order velocity moment $\langle U^3 \rangle$. This is in agreement with the earlier results of Al-Salem (1993) and Dohmen-Janssen et al. (2002).

4.2. Grain-size effect on net transport rates

All measured net transport rates from the LOWT experiments with asymmetric waves and uniform sand (Tables 5–8) are plotted together in Fig. 6 to study possible grain-size effects. All these data were collected under similar 2nd-order Stokes waves with almost the same degree of asymmetry R=0.65 but using the four different uniform sands (D=0.13, 0.21, 0.34 and 0.97 mm). It is shown that the sands with grain size ≥ 0.21 mm are always transported 'onshore', i.e. in the direction of the maximum crest velocity. The earlier finding of Al-Salem (1993) for D=0.21 mm ($\langle q_s \rangle \sim \langle U^3 \rangle$) appears to hold also for larger grain sizes and no clear grain-size influence is visible. Fine grains (D=0.13 mm) however show a strongly deviating behaviour. Measured net transport rates are 'onshore'

Table 7
Measured net transport rates of series B and C with uniform sand (D_{50}=0.21 mm)

Test	T (s)	U_{laser} (m/s)			$\langle U^3 \rangle$ (m³/s³)	$q_s \pm \sigma$ (10^{-6} m²/s)
		U_c	U_t	U_{rms}		
B7	6.5	0.95	0.5	0.5	0.102	12.42 ± 0.94
B8		1.31	0.7	0.7	0.256	38.85 ± 2.34
B9		1.72	0.86	0.92	0.562	69.83 ± 4.73
C1	6.5	1.07	0.57	0.55	0.121	18.74 ± 2.53
C2		1.11	0.54	0.55	0.152	25.54 ± 0.89
C9		1.05	0.66	0.56	0.115	20.46 ± 1.14
C11		1.39	0.87	0.8	0.276	51.47 ± 2.36

Table 8
Measured net transport rates of series D with uniform sand ($D_{50}=0.13$ mm)

Test	T (s)	U_{laser} (m/s)			$\langle U^3 \rangle$ (m³/s³)	$q_s \pm \sigma$ (10⁻⁶ m²/s)
		U_c	U_t	U_{rms}		
D11	6.5	1.0	0.59	0.56	0.096	9.0 ± 3.5
D12		1.6	0.94	0.91	0.537	-228.3 ± 25.75
D13		1.3	0.76	0.73	0.220	-30.2 ± 6.82
D14		0.79	0.48	0.45	0.044	7.6 ± 1.55

directed in the lower velocity regime ($\langle U^3 \rangle < 0.1$ m³/s³) but 'offshore' directed in the higher velocity regime ($\langle U^3 \rangle > 0.2$ m³/s³). Apparently, the assumption of quasi-steadiness (Al-Salem, 1993) does not always hold for the fine sand ($D < 0.21$ mm). For fine sands the settling time of sediment particles is no longer small in comparison with the duration of the half wave cycle (= ca. $T/2$), since these particles are stirred up to relatively high levels above the bed and also settle back to the bed more slowly (low settling velocity). The sediment concentration will lag substantially behind the velocity during the wave cycle (unsteady effects or phase-lag effects). In these conditions a part of the sediment stirred up during a wave cycle are still in suspension at flow reversal and will be transported in the opposite direction during the successive half-cycle. For asymmetric waves this effect will be much stronger for the 'onshore' half-cycle (with large velocities) than for the 'offshore' half-cycle and as a consequence net transport rates may be

reduced or may even change from 'onshore' to 'offshore'.

These phase-lag effects were studied experimentally in the LOWT before by Dohmen-Janssen et al. (2002) for sine waves superimposed on net currents and for different grain sizes in sheet-flow conditions. In these flow conditions net transport rates of fine grains ($D=0.13$ mm) are reduced when unsteady effects become more pronounced but they are still 'onshore' directed. It is also shown that in general phase-lag effects are expected to become important for large flow velocities, fine sands and small wave periods (see also the following section).

4.3. Time-dependent transport processes inside the sheet-flow layer

4.3.1. Time-dependent concentrations

The CCM measurements during series O provide insight in the time-dependent concentration behaviour during the wave cycle. As a typical example Fig. 7 shows ensemble-averaged concentrations at different phases during the wave cycle for different elevations above and inside the sheet-flow layer, as measured during experiment O4 (0.13 mm sand). The elevation $z=0$ is defined at the initial bed level before starting a test. The upper part of Fig. 7 shows the flow velocity above the boundary layer in the free stream ($z=100$ mm) measured by the LDA.
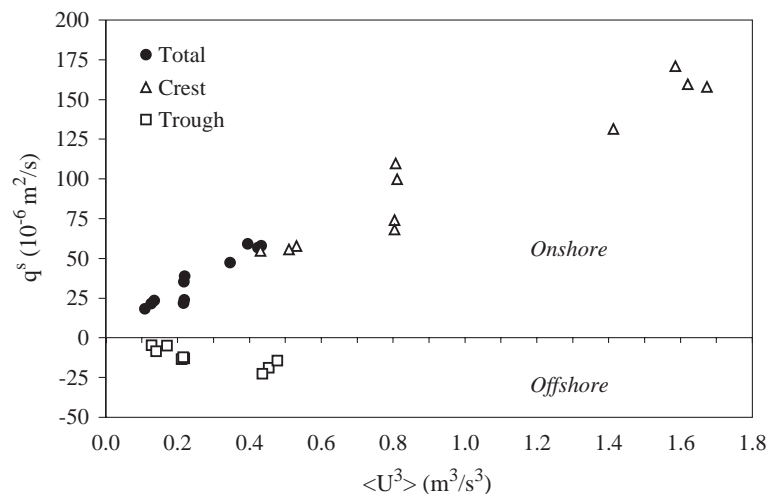

Fig. 5. Measured net transport rates as a function of the third-order velocity moment $\langle U^3 \rangle$ for series Q (uniform sand, $D=0.97$ mm).
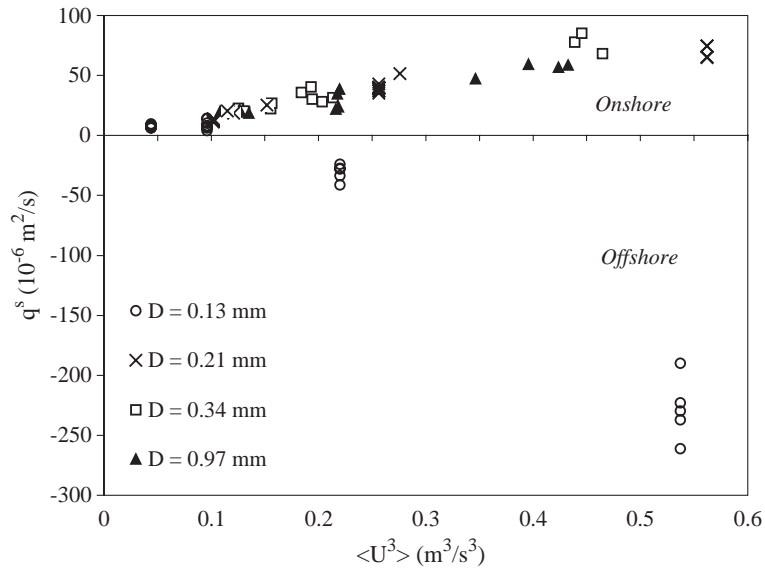
Fig. 6. Measured net transport rates as a function of the third-order velocity moment $\langle U^3 \rangle$ for uniform sands with different grain sizes.

In general, the measured time-dependent concentrations behave differently in the upper part and in the lower part of the sheet-flow layer, and two sub-layers can be distinguished (see also Ribberink and Al-Salem, 1995). The first layer is located between the non-movable sand up to $z = 0.0$ mm and is called the pick-up layer. The second layer, above the pick-up layer $z > 0.0$ mm is called the upper sheet-flow
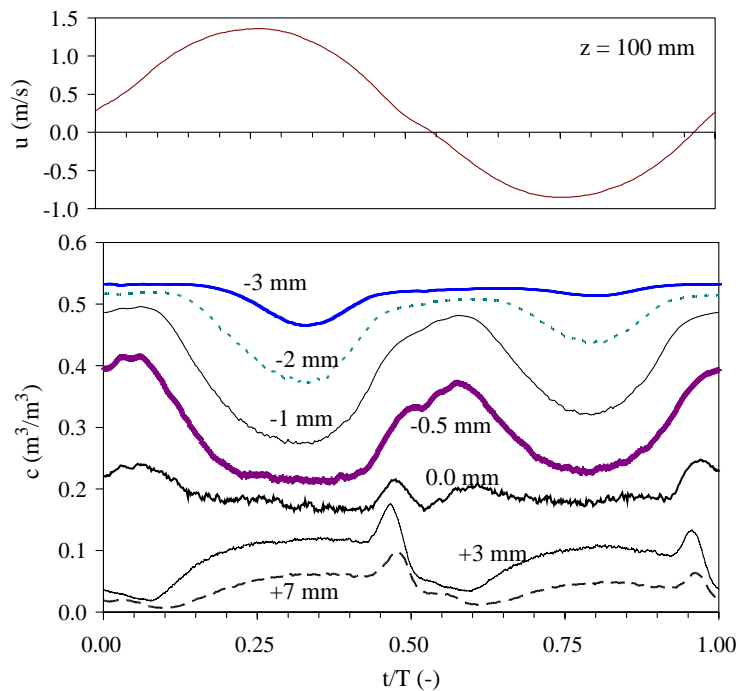
Fig. 7. Time-dependent sediment concentrations at different levels (mm) inside the sheet-flow layer, condition O4.
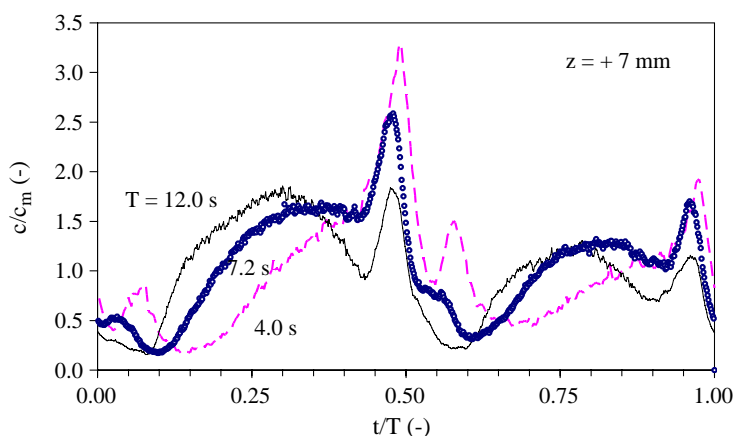
Fig. 8. Increasing phase-lags of sediment concentrations in the upper sheet-flow layer for decreasing wave periods ($z=+7$ mm).

layer. Due to vertical sediment exchange these two layers show opposite behaviour during the wave cycle. In the pick-up layer concentrations are decreasing when the velocity increases because sand particles are being picked-up from this layer and brought to higher levels in the flow. When the velocity decreases sand particles settle back to the bed and concentrations increase again. Opposite to this, in the upper sheet-flow layer concentrations increase for increasing velocity and decrease for decreasing velocity. In this upper layer concentration peaks are also observed just before flow reversal of the free stream. These peaks, which are not visible in the pick-up layer, were also observed during the experiments of Dohmen-Janssen et al. (2002) under sine waves superimposed on a net current and during asymmetric

wave experiments in different laboratory tunnels (e.g. Ribberink and Al-Salem, 1995; O'Donoghue and Wright, 2004). A possible physical explanation based on turbulence production and damping processes during flow acceleration and deceleration is given by Vittori (2003).

This observed intra-wave behaviour of the concentrations is strongly affected by the wave period. Fig. 8 shows ensemble-averaged concentrations as occurring in the upper sheet-flow layers at $z=+7$ mm above the bed for three wave periods (series O). Fig. 9 shows a similar comparison for wave periods at $z=-1$ mm in the pick-up layer. In both figures concentrations are normalized by the wave-averaged mean concentration c_m and time is normalized by the wave period T.

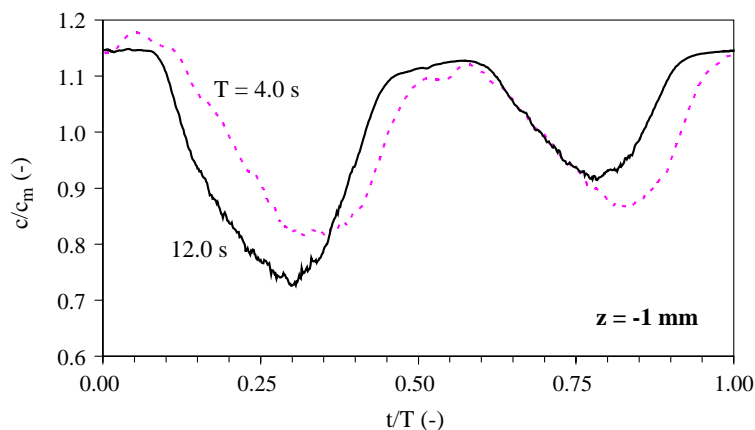

Fig. 9. Increasing phase-lags of sediment concentrations in the pick-up sheet-flow layer for decreasing wave periods ($z=-1.0$ mm).
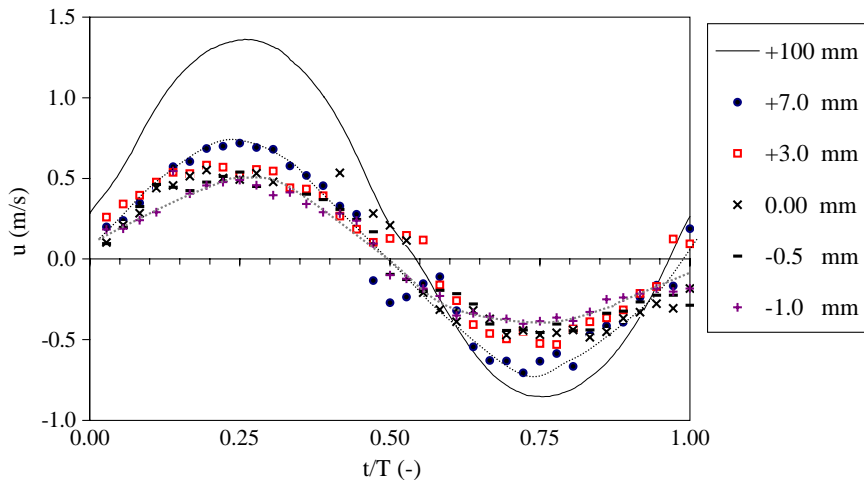
Fig. 10. Ensemble-averaged particle velocities at different levels inside the sheet-flow layer during experiment O4 (cross-correlation CCM technique).

In the long-period case (12 s), the concentration shows a more or less direct response to the time-dependent velocity variations during the wave cycle. However, for the shorter wave periods the concentrations showed a more delayed response (relative to the wave period) and increasing phase-lags can be observed for decreasing wave period. For example, Fig. 8 shows that for the long wave period (T=12.0 s) concentrations reach a maximum value during each half of the wave cycle which is then followed by a concentration reduction before the flow reversal. The extreme values are reached approximately at the same moment when the velocity also reaches its maximum value. For T=7.2 s, the maxima are reached much later but also the successive reduction in concentration is significantly less. For the shortest wave period T=4 s the concentration increase evolves again slower and the maximum value is not even reached before flow reversal. As a direct consequence of these phase-lag effects the sediment stirred up during one half wave cycle is not settled back to the bed

when the next half-cycle starts and may therefore contribute to the transport in opposite direction.

Similar phase-lags were observed earlier during oscillatory sheet flows with different grain sizes (finer sediment with smaller settling velocity shows more phase-lag) and form the explanation the fact that during waves with a superimposed current net transport rates may show a reduction when the grain size becomes smaller (see Dohmen-Janssen et al., 2002). The presently measured influence of the wave period confirms the idea that phase-lag effects are crucial for the magnitude of net transport rates under waves and currents.

4.3.2. Sand particle velocities

Fig. 10 shows measured time-dependent grain velocities in the sheet-flow layer against the wave phase, as obtained with the CCM cross-correlation technique for the same experiment O4. The solid line presents the measured velocities above the wave boundary layer (z=100 mm), measured by LDA. The other symbols represent velocities obtained at different ele-

Table 9
Measured net total transport rates of series P with graded sand (D_{50}=0.15 mm)

Test	T (s)	U_{laser} (m/s)			$\langle U^3 \rangle$ (m^3/s^3)	Net transport rate (10^{-6} m^2/s)		
		U_c	U_t	U_{rms}		Total $\pm \sigma$	(0.21 mm fraction)	(0.97 mm fraction)
P1	6.5	1.08	0.57	0.59	0.147	19.5 $\pm$ 2.4	11.2	8.39
P2		1.23	0.64	0.64	0.221	30.5 $\pm$ 4.4	16.47	14.03
P3		1.59	0.85	0.85	0.473	64.3 $\pm$ 6.9	29.9	34.4

Table 10
Measured net total transport rates of series S with graded sand ($D_{50}=0.24$ mm)

Test	T (s)	U_{laser} (m/s)			$\langle U^3 \rangle$ (m³/s³)	Net transport rate (10^{-6} m²/s)			
		U_c	U_t	U_{rms}		Total $\pm \sigma$	(0.13 mm fraction)	(0.34 mm fraction)	(0.97 mm fraction)
S1	6.5	0.87	0.45	0.45	0.070	10.4 ± 1.5	2.32	2.94	5.90
S2		1.14	0.57	0.61	0.168	19.0 ± 2.5	5.31	4.12	7.93
S3		1.30	0.65	0.70	0.261	22.4 ± 2.9	8.25	4.42	10.26
S4		1.63	0.82	0.90	0.535	15.40 ± 12.4	-9.80	6.80	18.40
S5	12.0	1.17	0.67	0.67	0.179	20.8 ± 3.9	8.54	4.23	8.04

vations (mm) above the initial sand bed, inside the sheet-flow layer.

The measured velocities are nearly sinusoidal, and have amplitudes decreasing with distance from bed. The measured velocities show some scatter around the moments of flow reversal, which is probably caused by the concentration-peaks which are generated in this wave phase (vertical sand motion instead of horizontal motion). It is clear that the reduction of the distance between the two CCM sensors to 11 mm (instead of 20 mm as used before by McLean et al., 2001) improved the cross-correlation technique. The smaller distance between the two sensors made the technique suitable for measuring the velocities during the complete wave cycle including the smaller velocities in the pick-up layer.

5. Results of the non-uniform sand experiments

Tables 9, 10 and 11 give the measured net total transport rates and the net transport rates of each size fraction of all experiments with non-uniform sands. Free-stream velocity characteristics at 100 mm above the bed are also included in these tables. These data include series P (mixture of 0.21 and 0.97 mm sand), S (mixture of 0.13, 0.34 and 0.97 mm sand) and series K (mixture of 0.13 and 0.32 mm sand).

5.1. Net total transport rates of non-uniform sand

Fig. 11 shows the measured net total transport rates as measured during series P, S and K as a function of the third-order velocity moment $\langle U^3 \rangle$. The net sand transport rates for all conditions of series P are positive, i.e. in the direction of the flow during the wave crest half-cycle ('onshore'). The sand transport rates again follow the 'quasi-steady' power law formulation $\langle q_s \rangle \sim \langle U^3 \rangle$ over the used velocity range. The net sand transport rates during series K and S also follow this power law but only in the low velocity regime $\langle U^3 \rangle < 0.2$. It is invalid in the high velocity regime ($\langle U^3 \rangle > 0.2$ m³/s³), probably due to unsteady effects of the fine size fraction ($D=0.13$ mm), which was strongly present in the used sand mixtures (60% of the mixture S and 50% of the mixture K; see below).

The net sand transport rates for each individual test show a relatively small deviation around their mean value, except for the highest velocity in series S (where $\langle U^3 \rangle > 0.5$ m³/s³). The latter is due to the fact in this particular case that it is high ($U_{rms} = 0.9$ m/s), the net transport rates are strongly affected by phase-lag effects and reach values close to zero. In this regime, the results are sensitive to small variations in the conditions (sand bed composition, flow velocity).

Table 11
Measured net total transport rates of series K with graded sand ($D_{50}=0.19$ mm)

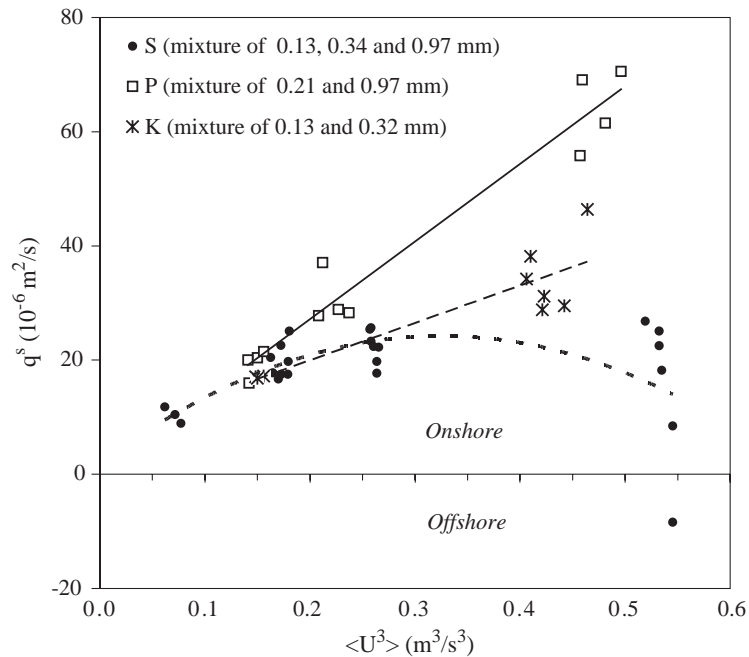| Test	T (s)	U_{laser} (m/s)			$\langle U^3 \rangle$ (m³/s³)	Net transport rate (10^{-6} m²/s)		
		U_c	U_t	U_{rms}		Total $\pm \sigma$	Fine (0.21 mm)	Coarse (0.34 mm)
K1	6.5	1.54	0.78	0.84	0.43	35.2 ± 9.4	-1.8	37.2
K2		1.10	0.55	0.58	0.151	17.4 ± 0.21	4.0	13.4

Fig. 11. Measured net total transport rates as a function of the third-order velocity moment $\langle U^3 \rangle$ for non-uniform sand experiments.

5.2. Total net transport rates of 'non-uniform' and 'uniform' sands

Fig. 12 shows a comparison between measured net total transport rates of a sediment mixture of two fractions (series P: mixture of 0.21 and 0.97 mm sand) and of the same fractions as single 'uniform' sand (series B/C: 0.21 mm and series Q: 0.97 mm). It is shown that the sediment mixture shows similar 'onshore' net transport rates as the uniform sands and apparently size-gradation have no clear effect.

A similar comparison is shown in Fig. 13 for the sediment mixture of series S (mixture of 0.13, 0.34 and 0.97 mm sand). The 'uniform' sand experiments are series D (0.13 mm), series R (0.34 mm) and series Q (0.97 mm). The dashed line in Fig. 13 shows the general trend of the measured net transport rates in case of the sediment mixture. In the low flow velocity regime ($\langle U^3 \rangle < 0.15$ m^3/s^3) the measured net transport rates of uniform sands and the sand mixture S are quite similar. However, in the higher velocity regime ($\langle U^3 \rangle > 0.15$ m^3/s^3), the measured transport rates of the mixed sand S are deviating from the single uniform sands. Although, the

sand mixture S has a median diameter ($D_{50} = 0.15$ mm) close to that of the uniform fine sand ($D_{50} = 0.13$ mm), the net transport rates show large differences. Apparently, the presence of coarse grains leads to a strong shift of the net transport rates in the positive 'onshore' direction. In these conditions it is likely that coarse grains in the mixture have the tendency to be transported in the 'onshore' direction, while the finest grains (0.13 mm) are transported in the 'offshore' direction. The result is a net total transport rate close to zero.

5.3. Net transport rates of size fractions in a mixture

The behaviour of the individual fractions of a mixture could be studied using the PBLT results. Fig. 14 shows the measured net total transport rates of the two fractions of series P versus the third-order moment of the flow velocity $\langle U^3 \rangle$. Similar to the behaviour of the single uniform sands, also in the mixture the net transport rates of both sizes are positive ('onshore' directed) and are increasing for increasing flow velocity. However, the net transport rates of both fractions are almost equal (50/50%), which is remarkable since the proportion of both
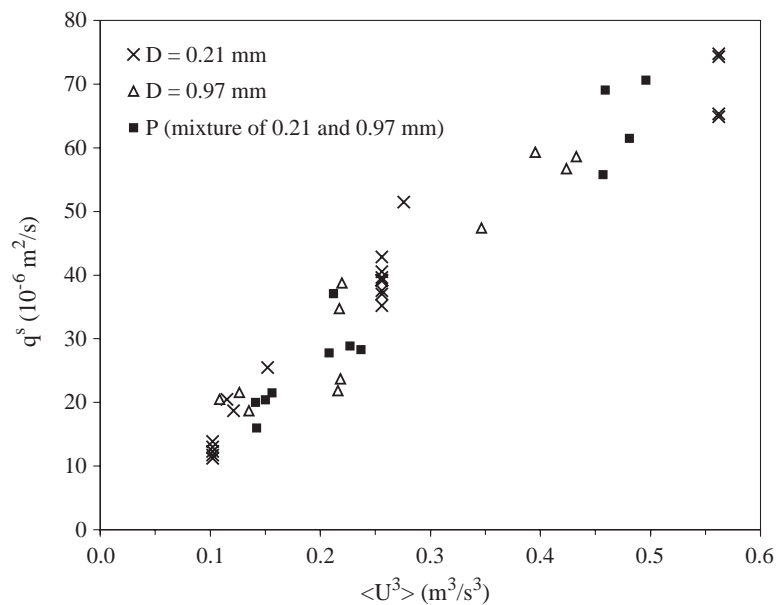
Fig. 12. Comparison between measured net total transport rates of two uniform sands (0.21 and 0.97 mm) and a mixture of these two sands (series P), as a function of the third-order velocity moment $\langle U^3 \rangle$.
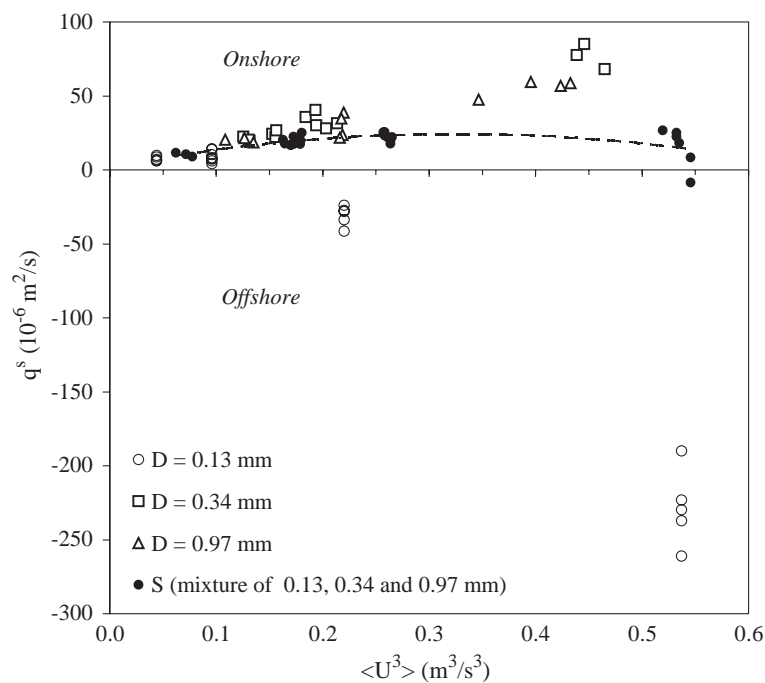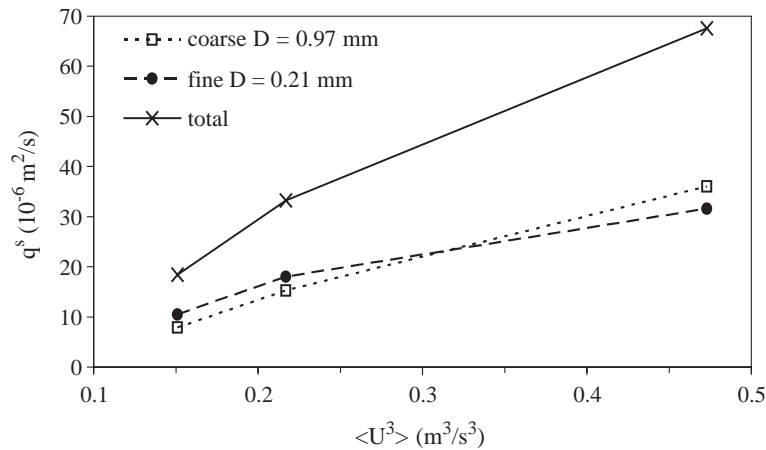

Fig. 13. Comparison between measured net total transport rates of three uniform sands (0.13, 0.34 and 0.97 mm) and of a mixture of these three sands (series S), as a function of the third-order velocity moment $\langle U^3 \rangle$.

Fig. 14. Measured net total transport rates and transport rates of each size fraction as a function of $\langle U^3 \rangle$ (series P).

size fractions in the original sand mixture is 70/30% (70% medium size 0.21 mm and 30% coarse size 0.97 mm). Apparently, selective transport processes occur, increasing the contribution of the coarse size and decreasing the contribution of the fine size. At higher flow velocities the share of the coarse fraction in the net total transport rate seems to increase even more. Selective transport can be related to various (vertical) sorting processes in the sheet-flow layer (see Section 5.5).

Similar selective processes were observed during the series S experiments (Fig. 15). However, the picture is more complex now since the selection pro-

cesses are taking place simultaneously with the phase-lag effects. It is shown that, due to a strong reduction of the transport of the finer sizes in the high-velocity regime, the net total transport rates now show a maximum for $\langle U^3 \rangle \approx 0.25$ m^3/s^3 and a decreasing trend for higher velocities. However, also now a similar selective transport process occurs, since the share of the coarse size in the net transport rate (40–80%) is always much larger than the share of the coarse size in the original sand bed (20%). Note that in Fig. 15 for series S the term 'fine fraction' refers to the finest size ($D=0.13$ mm) and the medium size ($D=0.34$ mm) together.
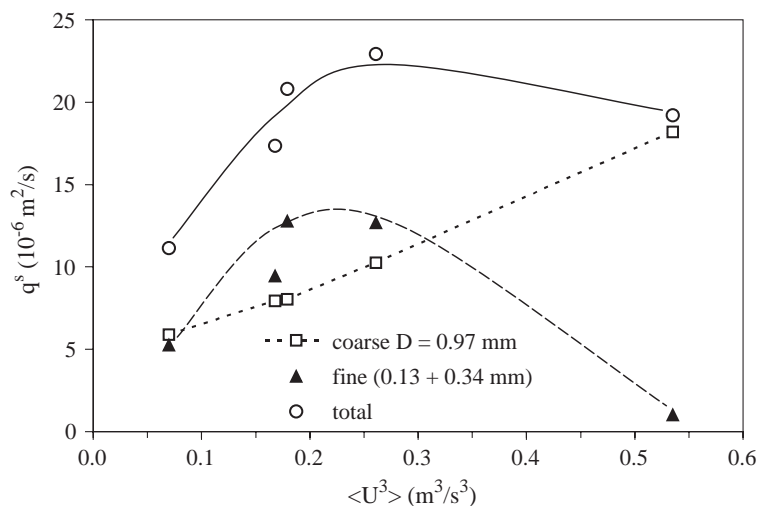

Fig. 15. Measured net total transport rates and net transport rates of each size fraction as a function of $\langle U^3 \rangle$ (series S).
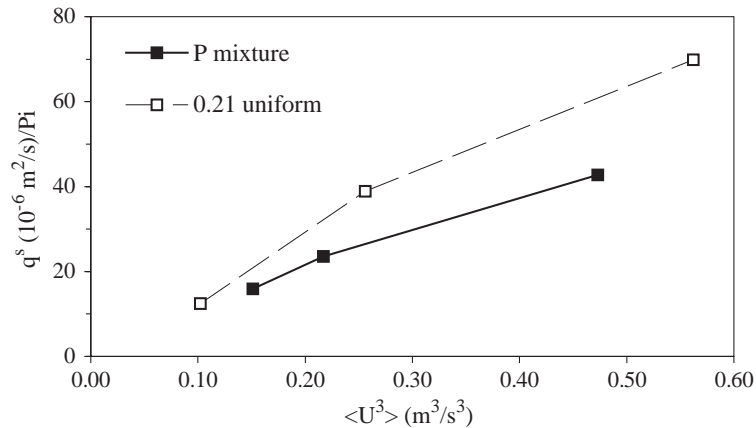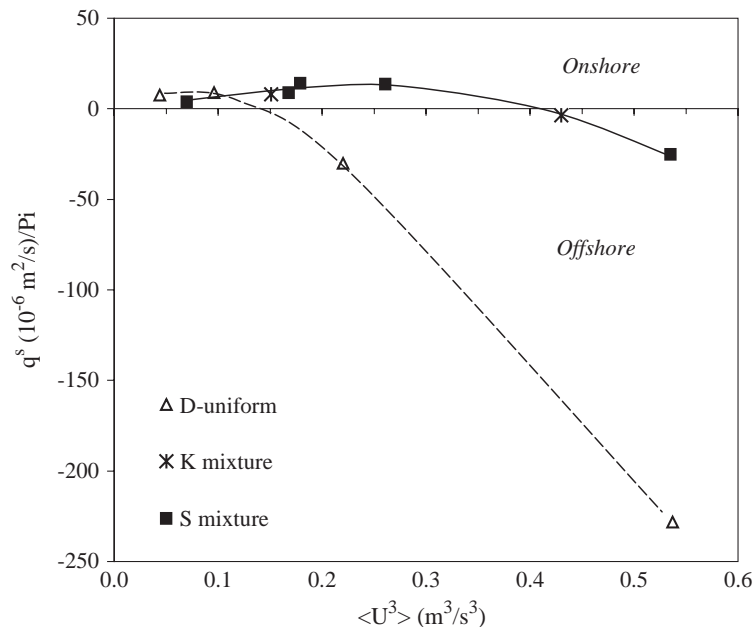
Fig. 16. Comparison between measured net transport rates of medium sand (0.21 mm) being part of a coarser mixture (series P) and in a 'uniform medium sand' situation.

5.4. Interaction between grain sizes in a mixture

In order to study the interaction between different grain sizes in mixtures in some more detail, the measured transport rates of individual sizes in a mixture are compared with the transport rates of the same sizes in case of uniform sand for the same hydraulic conditions. To account for the reduced presence of the size fractions in the sand bed in the mixture situation, the fractional transport rates $q_{s,i}$ are divided by their probability of occurrence p_i in the original sand mixture.

First two cases are shown of fine grains being part of a coarser mixture. Fig. 16 shows a comparison of measured transport rates of medium sand ($D = 0.21$ mm), (i) in the situation of being part of a mixture (series P, mixed with the coarser 0.97 mm

Fig. 17. Comparison between measured net transport rates of fine sand (0.13 mm) being part of a coarser mixture (series K and S) and in a 'uniform fine sand' situation.

sand), and (ii) in the situation of being transported as single uniform sand (series B and C). It is shown that in a relative sense (after accounting for the difference in volume percentage p_i), the 0.21-mm size is transported with lower rates in case of being mixed with a coarser size than in a 'uniform material' situation. The reduction in transport rates is somewhat more pronounced at higher velocities ($\langle U^3 \rangle > 0.25$ m^3/s^3).

Fig. 17 shows a similar comparison for a fine sand size ($D = 0.13$ mm) as part of a coarser mixture (series K and S) and in the 'uniform material' situation (series D). In series K the fine sand ($D = 0.13$ mm) was mixed with 0.32 mm sand, while in series S the fine sand was mixed with 0.34 and 0.97 mm sands. It is observed that the strong negative ('offshore' directed) net transport rates of the 'uniform' fine sand do not occur in the mixture situation. Moreover, the transition from 'onshore' to 'offshore' is shifted to higher velocities due to the interaction with the coarser grains in the mixtures.

In both cases the mobility of the finer fraction(s) in the mixture seems to have been reduced, due to the presence of coarser sizes in the mixture. This leads to reduced transport rates (absolute magnitudes). This reduced mobility of finer fractions in a coarser mixture is also observed in uni-directional flows (e.g. river flows; see, e.g. Wilcock and McArdell, 1993; Ribberink et al., 2002). In these conditions, with plane beds and with dune bedforms, the reduced mobility is caused by reduced exposure to the flow ('hiding' effects).

Although not directly measured in this study, it is likely that the reduced mobility also leads to reduced entrainment heights above the bed of the fine sand fraction and consequently reduced phase-lags. This would explain the fine sand behaviour in the high-velocity regime in Fig. 17.

Similar but opposite effects occur for a coarse size being part of a finer mixture. In Fig. 18 a comparison is presented between measured net transport rates of a 'uniform' coarse size ($D = 0.97$ mm, series Q) and of the same coarse fraction in finer sand mixtures (series P and S). For all flow conditions the transport rates of the coarse sand are larger when they are part of a sand mixture than in the 'uniform coarse sand' situation. Apparently, the coarse sand experiences an increase in mobility when being part of a finer mixture. Also this is consistent with earlier uni-directional flow observations (increased flow exposure).

Although exposure effects seem to be similar for oscillatory sheet flows and for uni-directional flows, their effect on horizontal sorting (due to selective transport of sizes) may work out differently. In Fig. 19 selective transport of sizes is visualized by plotting the probability of each size fraction in transported sand ($p_{i\_\text{trans.}}$) scaled by its probability in the original sand mixture (p_{i_original}) as a function of D_i/D_m. Herein D_i is the diameter of each size fraction and D_m is the mean diameter ($= \sum p_i D_i$). Fig. 19 shows this relation on a log-linear scale for all non-uniform
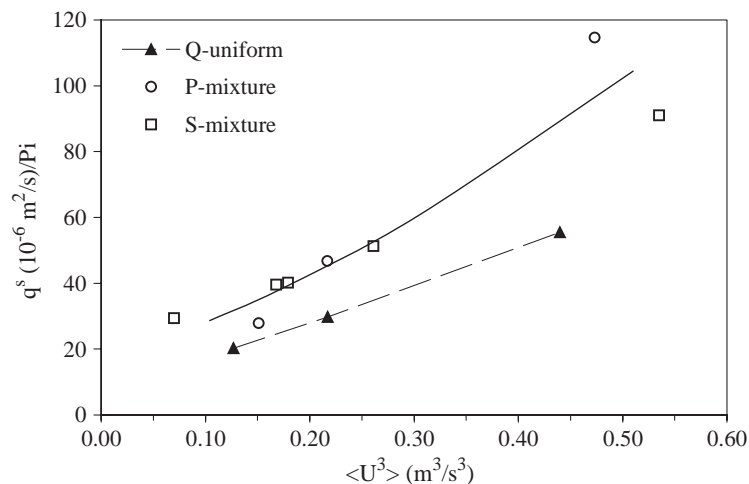

Fig. 18. Comparison between measured net transport rates of coarse sand (0.97 mm) being part of a finer mixture (series P and S) and in a 'uniform coarse sand' situation.
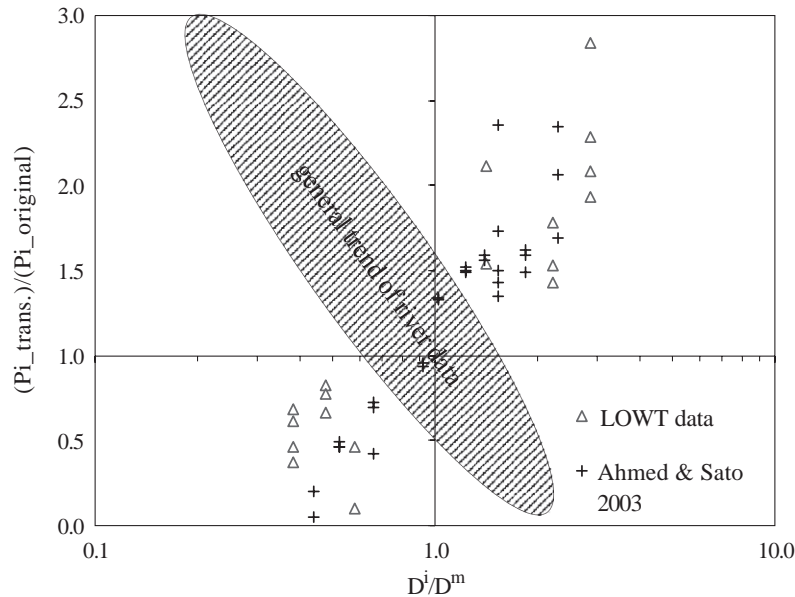
Fig. 19. Relation between $(p_{i\_\text{trans.}})/(p_{i\_\text{original}})$ and (D_i/D_m).

sand experiments in the LOWT (present work) in combination with new non-uniform sand data of Ahmed and Sato (2003). The latter experiments were carried out in the oscillating water tunnel of Tokyo University with relatively small wave periods ($T=3.0$ s) using sand mixtures consisting of three different sand sizes (0.21, 0.49 and 0.74 mm). Both datasets agree with each other and show that the coarse fractions of a mixture ($D_i/D_m>1$) always contribute more to the total transport rate than would be expected from their volume share in the original sand mixture ($p_{i\_\text{trans}}/p_{i\_\text{bed}}>1$). Fine grains ($D_i/D_m<1$) however always contribute less to the total transport rate ($p_{i\_\text{trans}}/p_{i\_\text{bed}}<1$). This result is opposite to selective sand transport in uni-directional flows (e.g. Wilcock and McArdell, 1993; Wilcock et al., 2001). Here finer sizes generally still contribute more than coarser sizes to the total transport rate, despite the equalizing effect of exposure processes. The general trend of the size-selective processes in uni-directional flows is shown in Fig. 19 by the hatched area.

5.5. Sorting processes of grain sizes

The selective behaviour of size fractions in a mixture and the interaction between size fractions goes hand in hand with vertical sorting processes in the bed, in the sheet-flow layer and in the suspension layer. Grain-size analysis of samples taken from the bed, from the PBLT (sheet-flow layer) and from the TSS measurements (suspension layer) provide insight in these processes.

Time-averaged suspended concentrations were measured during series P and S (sand mixture experiments) using a transverse suction system (TSS). Grain-size analysis of the TSS samples shows that only the smallest sizes of the sand mixture go into suspension. Fig. 20 shows the vertical distribution of D_{50} for the three different wave conditions of series P. Even at the lowest level near the bed $D_{50}<0.175$ mm, indicating that only the smaller particles of the finest fraction of the mixture go into suspension (D_{50} of the finest fraction$=0.21$ mm). The grain size of the suspended sediment becomes smaller as the distance above the bed increases (vertical sorting). Moreover, as the flow velocity (U_{rms}) increases, the suspended sediment at all elevations becomes somewhat coarser.

Grain-size analysis of PBLT samples provides insight in the grain-size composition of the 'onshore' and 'offshore' transport taking place inside the sheet-flow layer. Fig. 21 shows the percentage of the coarse fraction in the transported sand during both the 'onshore'
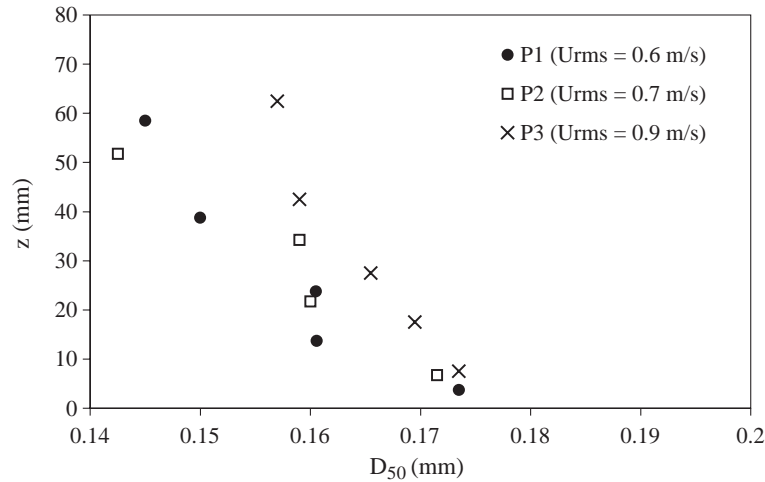
Fig. 20. Vertical distribution of D_{50} of suspended sediment for three flow conditions (series P).

and 'offshore' half wave cycle as a function of the corresponding peak velocity (U_c = 'onshore' crest velocity, U_t = 'offshore' trough velocity). Since the two experimental series with graded sand (S and P) show the same trend, Fig. 21 shows only the results of series P. More details can be found in Hassan et al. (1999, 2002).

It is shown that the transported sediment is always coarser (35–50% coarse fraction) than the original sand mixture (30% coarse). Moreover, the contribution of the coarse fraction in the transported material increases

with increasing velocity amplitude. The 'onshore' transport with higher peak velocities is generally coarser than the transport during the 'offshore' wave motion.

Samples taken from the bed after a tunnel test provide additional insight in vertical sorting in the upper centimeters of the bed. Since series P and S show more or less the same vertical sorting trend in the upper bed layer, only the results of series P will be discussed here. Fig. 22 shows the average distribution of the percentage of coarse fraction against depth, for two conditions (P1 and P3). These grain-size distributions are
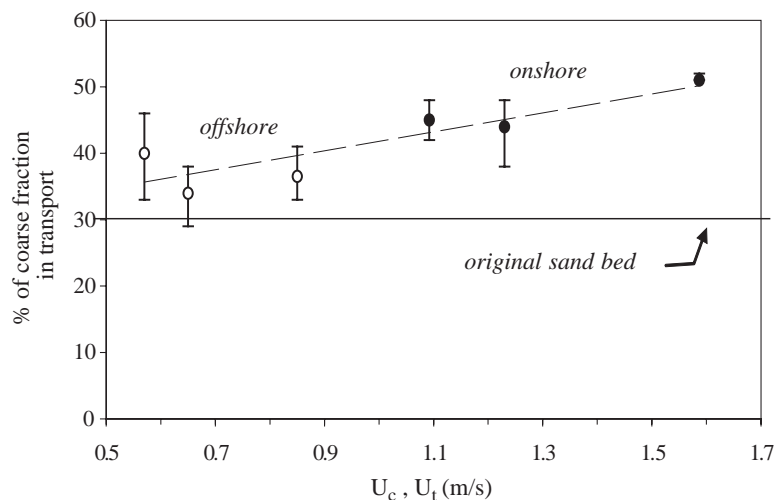

Fig. 21. 'Onshore' and 'offshore' bed-load compositions versus peak velocities (U_c,U_t), measured by PBLT during series P (● = 'onshore', ○ = 'offshore').
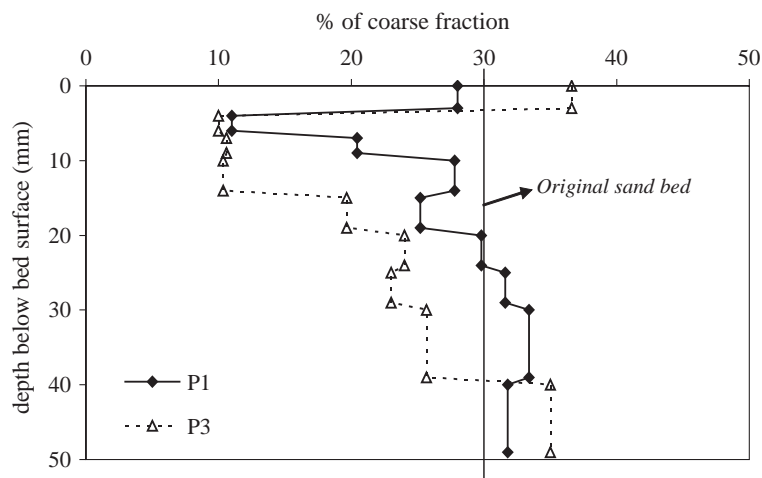
Fig. 22. Distribution of the percentage of coarse fraction with depth below the bed surface, showing relatively fine sediment layers below a coarser bed surface (series P).

an average result of samples taken at 3 to 5 locations along the tunnel for several tunnel tests. It is shown that the bed composition after a tunnel test is no longer uniform with depth and vertical sorting has occurred. The top millimeters of the bed have roughly the same composition as before the test (=30% coarse sand). However, below this top layer a layer has formed of about 5–20 mm thick containing relatively more fine sand (10–20% coarse sand). At larger depths the composition of the bed seems to be undisturbed by the experiment. The thickness of the disturbed or active bed layer increases with increasing velocity. For condition P1 the 'active layer' is about 20 mm thick, for condition P3 about 30 mm. This active layer is the resulting bed structure after a tunnel test and therefore includes the effect of small mean bed-level changes which occur in the test section during the complete test. Consequently this layer is much thicker than the instantaneous erosion depth of only a few millimeters (below the mean bed level) occurring during one wave cycle.

On the average, this result shows that the upper bed layers became finer during a test. This occurs for each of the two wave conditions and is in accordance with the relatively coarse composition of the sand collected in the sand traps (contains more than 30% coarse sand fraction). During the experiment the coarse fraction is slowly washed out from the upper layers of the bed. The presence of an upper coarse layer confirms the idea that coarse grains are brought upwards in some

way, become more exposed to the flow and become therefore more mobile in a mixture. Kinematic sorting may explain the observed sorting in the upper bed layer (Legros, 2002). This type of sorting is related to the relative size differences between grains in a mixture being in motion. Under the effect of oscillatory motion (or shaking) the pore space between grains is increased because the sand grains push neighboring grains away. Consequently, small grains tend to move downwards between the large grains which at the same time move upwards, irrespective of their weight (see also Kleinhans, 2004).

6. Conclusions

Full-scale experiments were carried out in the Large Oscillating Water Tunnel of WL|Delft Hydraulics to gain a better understanding of size-selective sediment transport processes under oscillatory plane-bed/sheet-flow conditions.

'Uniform sand' experiments showed that, for sand sizes between $0.2 < D < 1.0$ mm, net transport rates under 2nd-order Stokes waves are not affected by the grain size and show the same direct proportionality with the third-order velocity moment $\langle U^3 \rangle$. Meanwhile, a finer sand ($D = 0.13$ mm) shows a different behaviour in the high velocity range, i.e. for $U_{rms} > 0.6$ m/s. In this regime net sand transport rates change

from the 'onshore' direction into the 'offshore' direction due to the presence of unsteady (or phase-lag) effects. The assumption of quasi-steadiness of the intra-wave transport process (Ribberink and Al-Salem, 1994) does no longer hold.

Time-dependent measurements of sand concentrations with CCM provided new insights into these phase-lag effects inside the sheet-flow layer (0.13 mm sand). For relatively long waves ($T=12.0$ s) the concentrations are nearly in phase with the time-dependent flow velocity variations during the wave cycle. Meanwhile, for shorter wave periods (7.2 and 4.0 s) increasing phase-lags are observed and the intra-wave transport processes become more non-quasi-steady. The sediment entrainment from the bed as well as the deposition process back to the bed lags behind the wave motion more and more. In this way sediment stirred up during one half wave cycle becomes more and more available for transport in opposite direction during the next half wave cycle. These observed phase-lag effects are responsible for the reduced 'onshore' and the 'offshore' directed net transport rates of the 0.13 mm sand.

During the experiments a new cross-correlation technique with two CCM sensors for measuring sediment velocities inside the sheet-flow layer was developed further. Particle velocities could now be measured during the complete wave cycle throughout the sheet-flow layer by reducing the distance between two CCM sensors (to 11 mm instead of 20 mm). The particle velocities showed a small phase-lead with respect to the free-stream oscillatory flow were more or less sinusoidal and showed a small reduction in amplitude when approaching the bed form +10 mm to −1 mm.

'Graded sand' experiments showed that size-gradation has almost no effect on the net total transport rates, provided that the grain sizes of the sand mixture are in the range $0.2 < D < 1.0$ mm. However, if a substantial fraction of fine grains ($D = 0.13$ mm) is present in the mixture, net transport rates of graded sand may be different from those of uniform sand (with the same D_{50}) depending on the flow velocity regime. All mixture experiments showed the presence of important size-fraction interactions. Fine fractions show relatively lower net transport rates when being part of a (coarser) mixture than in the 'uniform fine-sand' situation, while the opposite occurs for coarse fractions in a (finer) mixture. The relative contribution of the coarse grains to the total transport is therefore larger than would be expected based on their volume proportion in the original sand mixture (selective transport of coarser sizes).

Differences in entrainment and mixing characteristics of grain sizes lead to vertical segregation of sizes in the near-bed transport layers (e.g. fines more in suspension and coarse sizes in the bed-load layer). The finer fractions in a mixture therefore experience stronger time-history effects during a wave cycle than the coarser sizes, which show a more 'quasi-steady' transport behaviour. During asymmetric waves this selective behaviour of sizes generally invokes a net 'onshore' motion of coarse sizes, and at the same time a much smaller net 'onshore' or even net 'offshore' motion of finer sizes (in the high velocity regime). Kinematic sorting of sizes (upward motion of coarse sizes and downward motion of fines) may be responsible for a relatively large flow exposure and mobility of the coarse grains, which also occurs for lower velocities. Bed samples showed the presence of a relatively fine sediment layer (10–20 mm thick) below a few millimetres thick coarser surface layer.

Acknowledgements

References

Ahmed, A.S.M., Sato, S., 2003. A sheetflow transport model for asymmetric oscillatory flows: Part II. Mixed grain size sediments. Coast. Eng. J. JSCE 45 (3), 339–361.

Al-Salem, A.A., 1993. Sediment transport in oscillatory boundary layers under sheet flow conditions. PhD Thesis, Delft Univ. of Technology, The Netherlands.

Blom, A., Ribberink, J.S., de Vriend, H.J., 2003. Vertical sorting in dunes—flume experiments with a natural and a tri-modal sediment mixture. Water Resour. Res. 39 (2), 1025. doi: 10.1029/2001WR001088.

Bosman, J.J., van der Velden, E.T.J.M., Hulsbergen, C.H., 1987. Sediment concentration measurement by transverse suction. Coast. Eng., 11.

Dean, R.G., 1991. Equilibrium beach profiles. J. Coast. Res. 7 (1), 53–84.

Dibajnia, M., Watanabe, A., 1992. Sheet flow under nonlinear waves and currents. Proc. of the 23rd Int. Conf. on Coast. Eng., Venice, pp. 2015–2028.

Dibajnia, M., Watanabe, A., 1996. A transport rate formula for mixed-size sands. Proc. of the 25th Int. Conf. on Coast. Eng., Orlando, pp. 3791–3803.

Dibajnia, M., Watanabe, A., 2000. Moving layer thickness and transport rate of graded sediment. Proc. of the 27th ICCE. ASCE, pp. 2752–2765.

Dohmen-Janssen, C.M., Hassan, W.N.M., Ribberink, J.S., 2001. Mobile-bed effects in oscillatory sheet flow. J. Geophys. Res. 106 (C11), 27103–27115.

Dohmen-Janssen, C.M., Kroekenstoel, D.F., Hassan, W.N.M., Ribberink, J.S., 2002. Phase-lags in oscillatory sheet flow: experiments and bed load modelling. J. Coast. Eng. 46, 61–87.

Guillen, J., Hoekstra, P., 1997. Sediment distribution in the near-shore zone: grain size evolution in response to shoreface nourishment (Island of terschelling, The Netherlands). Estuar., Coast. Shelf Sci. 45, 639–652.

Hassan, W.N.M., 2001. Sand transport processes in oscillatory sheet flows with different wave periods—CCM measurements in the large oscillating water tunnel. MICS Report 2001W-002. Civil Eng. and Management, Univ. of Twente, The Netherlands.

Hassan, W.N.M., 2003. Transport of size-graded and uniform sediments under oscillatory sheet-flow conditions. PhD Thesis, Univ. of Twente, The Netherlands, ISBN 90-365-1889-x.

Hassan, W.N.M., Kroekenstoel, D.F., Ribberink, J.S., van Rijn, L.C., 1999. Gradation effects on sand transport under oscillatory sheet-flow conditions. Research report, WL/Delft Hydraulics and Univ. of Twente, The Netherlands, 165 pp.

Hassan, W.N.M., van der Scheer, P., Ribberink, J.S., 2002. Oscillatory flow experiments over flat sandy beds using coarse sand, medium sand and a sand mixture of coarse, medium and fine sand. Research report, WL/Delft Hydraulics and Univ. of Twente, The Netherlands.

Katoh, K., Yanagishima, S., 1995. Changes of sand grain distribution in surf zone. Coast. Dynamics, Gdansk, Poland, pp. 639–649.

King, D.B., 1991. Studies in oscillatory flow bedload sediment transport. PhD Thesis, Univ. of California, San Diego.

Kleinhans, M.G., 2004. Sorting in grain flows at the lee side of dunes. J. Earth Sci. 65, 75–102.

Klopman, G., 1994. Vertical structure of the flow due to waves and currents. Report H840.30: Part II. WL/Delft Hydraulics, The Netherlands.

Legros, F., 2002. Can dispersive pressure cause inverse grading in grain flows? J. Sediment. Res. 72, 166–170.

McLean, S.R., Ribberink, J.S., Dohmen-Janssen, C.M., Hassan, W.N.M., 2001. Sediment transport measurements within the sheet flow layer under waves and currents. J. Waterw., Port, Coast., Ocean Eng. (ISSN: 0733-950X).

O'Donoghue, T., Wright, S., 2004. Concentrations in oscillatory sheet flow for well sorted and graded sands. J. Coast. Eng. 50, 117–138.

Ribberink, J.S., Al-Salem, A.A., 1994. Sediment transport in oscillatory boundary layers in cases of rippled beds and sheet flow. J. Geophys. Res. 99 (C6), 12707–12,727.

Ribberink, J.S., Al-Salem, A.A., 1995. Sheet flow and suspension in oscillatory boundary layers. Coast. Eng. 25, 205–225.

Ribberink, J.S., Chen, Z., 1993. Sediment transport of fine sand under asymmetric oscillatory flow. Report H840: Part VII. January 1993, WL/Delft Hydraulics.

Ribberink, J.S., Blom, A., van der Scheer, P., van Straalen, M.P., 2002. Multi-fraction techniques for sediment transport and morphological modelling in sand–gravel rivers. In: Bousnar, Zech (Eds.), Proc. of River Flow Conference, pp. 731–740.

Van Rijn, L.C., 1997a. Sand transport and bed composition along cross-shore profile. Coastal Dynamics '97, Plymouth, England, pp. 88–98.

Van Rijn, L.C., 1997b. Calibration of mechanical bed load transport sampler. Note, WL/Delft Hydraulics, The Netherlands.

Vittori, G., 2003. Sediment suspension due to waves. J. Geophys. Res. 108 (C6), 3173.

Watanabe, A., Sato, S., 2002. A sheet-flow transport rate formula for mixed-size sands in compound oscillatory-steady flow. Proc. of the 28th ICCE. ASCE, pp. 3033–3045.

Wilcock, P.R., 1993. Critical shear stress of natural sediments. J. Hydraul. Eng. 119 (4), 491–505.

Wilcock, P.R., McArdell, B., 1993. Surface-based fractional transport rates: mobilization thresholds and partial transport of a sand–gravel sediment. J. Water Resour. Res. 29 (4), 1297–1312.

Wilcock, P.R., Kenworthy, S.T., Crowe, J.C., 2001. Experimental study of the transport of mixed sand and sand gravel. J. Water Resour. Res. 37 (12), 3349–3358.

Wilson, K.C., 1987. Analysis of bed-load motion at high shear stress. ASCE J. Hydraul. Eng. 113 (1), 97–103.

Zala Flores, N., Sleath, J.F.A., 1998. Mobile layer in oscillatory sheet-flow. J. Geophys. Res. 103 (C6), 12783–12793.